JOURNAL OF COMPUTATIONAL PHYSICS 90, 141–160 (1990)

The Behavior of Flux Difference Splitting Schemes near Slowly Moving Shock Waves*

THOMAS W. ROBERTS

FFA, the Aeronautical Research Institute of Sweden, P.O. Box 11021, S-161 11 Bromma, Sweden

Received July 28, 1988; revised March 28, 1989

An investigation of the behavior of shock capturing schemes which compute the numerical flux from a solution of Riemann's problem is performed. The schemes of Godunov, Roe, and Osher are examined for a one-dimensional model problem consisting of a nearly stationary shock. Both scalar and systems of equations are examined. It is found that for slow shocks there is a significant error generated when solving systems of equations, while the scalar results are well behaved. This error consists of a long wavelength noise in the downstream running wave families that is not effectively damped by the dissipation of the scheme. The source of this error is shown, and the implications for the performance of these schemes are considered. This error may contribute to the slow convergence to steady state reported by many researchers. © 1990 Academic Press, Inc.

1. INTRODUCTION

Recent years have seen tremendous progress in the development of numerical methods for solving the equations governing the unsteady flow of an inviscid, adiabatic ideal gas—the Euler equations. The difficulty in the numerical solution of the Euler equations arises primarily from their nonlinearity, in particular the mechanism that allows the formation of shocks. The most active area of research recently has been in the development of so-called "upwind" difference schemes; a general overview of such methods can be found in the review by Roe [1]. A recent survey by Woodward and Colella [2] compares a variety of methods for the computation of unsteady flows with strong shocks. Their results show that, at least for a particular class of higher order upwind schemes, significant improvements in accuracy and efficiency are obtained over conventional artificial viscosity methods. The type of upwind schemes that they consider are referred to as "flux difference splitting" schemes. These are also referred to as "Godunov-type" schemes, as the method of Godunov [3] is the original flux difference splitting scheme. These schemes have in common that the numerical flux is computed from either an exact or approximate solution of Riemann's problem at cell intefaces. Second-order

* This research was funded in part by FFA and in part by the National Swedish Board for Technical Development.

0021-9991/90 $3.00
Copyright © 1990 by Academic Press, Inc
All rights of reproduction in any form reserved.

accuracy or better is obtained by a nonlinear interpolation of either the fluxes or the dependent variables; the philosophy behind this approach is outlined by Roe [1] and Woodward and Colella [2].

The results shown by Woodward and Colella point out a source of error behind a shock that is nearly stationary, which occurs when using Godunov's method. Numerical noise is generated in the discrete shock transition layer and is transported downstream. The results in [2] illustrate that this error can have a significant global influence on the accuracy of the results. In addition, they show [4,2] that the source of this error is found in the first-order accurate version of Godunov's scheme and is not due to the interpolation procedure used to obtain higher order accuracy.

It is the object of this paper to examine the source of this error by considering three first-order accurate flux difference splitting schemes. A comparison of Godunov's [3], Roe's [5], and Osher's [6] upwind schemes is made for a one-dimensional flow consisting of a slowly moving shock wave. ("Slowly moving" means that the ratio of the shock speed to the maximum wave speed in the domain is $\ll 1$.) In their own high-order PPM method, Colella and Woodward [4] discuss the error in some detail and give a heuristic explanation of it. They also present additional numerical dissipation terms to damp it. It will be shown below that their explanation of the error is incomplete and that different schemes (i.e., different numerical flux formulas) have significantly different levels of this noise. This error is inherent to nonlinear systems of equations; solutions for scalar conservation laws are perfectly well behaved. It will also be pointed out that the use of total variation diminishing (TVD) concepts in the construction of higher order schemes accentuates the problem.

Although the present work is motivated by the author's interest in computing unsteady flows, this study may also have implications for steady flow computations. The interest in upwind schemes for steady flows is due to their extremely good resolution of steady shocks. These flux difference splitting algorithms are being used to compute steady flows in a time asymptotic fashion. The rate of convergence to the steady state is dominated by the slow propagation of the shocks to their equilibrium positions. Typically, higher order flux difference splitting schemes converge very slowly to the steady state, as reported by Lytton [7] and Yee [8], for example. (The author has also had this same experience with two-dimensional steady transonic calculations.) The error behind slow shocks examined here may be a contributing factor to this slow convergence.

The rest of the paper is organized as follows. In the next section, the equations of motion and the model problem are described. In Section 3, the three flux difference splitting methods are described. Results are presented in Section 4, and in Section 5 the observed behavior is explained in terms of the discrete shock structure. The paper is then summarized in the concluding section.

2. Equations and Model Problem

The flux difference splitting schemes mentioned above were compared for three sets of equations: the inviscid Burgers equation,

$$u_t + \left(\frac{1}{2}u^2\right)_x = 0; \tag{1}$$

the Euler equations for an isothermal gas,

$$\begin{aligned} \rho_t + (\rho u)_x &= 0, \\ (\rho u)_t + (\rho(u^2 + a^2))_x &= 0, \end{aligned} \tag{2}$$

where ρ is the density, u is the velocity, and a is the speed of sound, a constant; and the full Euler equations for an ideal gas with constant specific heats,

$$\begin{aligned} \rho_t + (\rho u)_x &= 0, \\ (\rho u)_t + (\rho u^2 + p)_x &= 0, \\ (\rho E)_t + ((\rho E + p)u)_x &= 0, \end{aligned} \tag{3}$$

where p is the pressure, $E = u^2/2 + p/((\gamma - 1)\rho)$ is the specific total energy, and γ is the specific heats ratio.

All the above equations are hyperbolic conservation laws, and may be written in the form

$$\frac{\partial \mathbf{U}}{\partial t} + \frac{\partial \mathbf{F}(\mathbf{U})}{\partial x} = 0, \tag{4}$$

where $\mathbf{U}$ is the state vector of the conserved variables and $\mathbf{F}(\mathbf{U})$ is the flux function. For the purpose of discussing the schemes under consideration in the next section, Eq. (4) is the most convenient form of the equations.

The model problem is shown in Fig. 1. Each equation was solved for a flow consisting of a single shock wave propagating slowly to the left. The initial

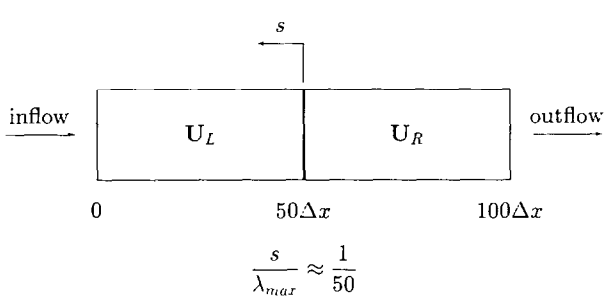

FIG. 1. Model problem for flux difference splitting.

conditions for each case consisted of two constant states separated by the exact shock jump at the midpoint of a domain of 100 cells. The states were chosen to give a ratio of the shock speed to the maximum eigenvalue of the system of about 1:50. In other words, at a Courant number of 1, the shock would traverse a single cell in approximately 50 time steps. All cases shown below were computed for a Courant number of 0.95; the results were insensitive to changes in this parameter.

The left (inflow) boundary was supersonic, so all flow variables were specified there. At the right (outflow) boundary, there was always one characteristic entering the domain. The appropriate characteristic variable was specified; its value was given by the exact postshock conditions. All remaining characteristic quantities were extrapolated.

3. Numerical Methods

The equations presented in the previous section were solved using first order accurate versions of Godunov's [3], Roe's [5], and Osher's [6] methods. All these schemes for solving Eq. (4) can be written in the form

$$\mathbf{U}_j^{n+1} = \mathbf{U}_j^n - \frac{\Delta t}{\Delta x}(\hat{\mathbf{F}}_{j+1/2}^n - \hat{\mathbf{F}}_{j-1/2}^n), \tag{5}$$

where j and n are the spatial and time level indices, and $\hat{\mathbf{F}}_{j+1/2}^n$ is the numerical flux function at the interface between cells j and $j+1$ at time level n. Depending on the choice of the numerical flux formula, Eq. (5) is referred to as Godunov's, Roe's, or Osher's, scheme. All three schemes are stable for a Courant number $\leqslant 1$.

The schemes considered here compute the numerical flux $\hat{\mathbf{F}}_{j+1/2}^n$ from either an exact or approximate solution of the Riemann problem at cell interfaces. How this is done is now described for each of the three schemes.

3.1. *Godunov's Scheme*

Godunov [3] first proposed the use of the Riemann problem for computing the numerical flux function in Eq. (5). If at time $t=0$, the flow consists of two constant states

$$\mathbf{U}(x<0, t=0) = \mathbf{U}_L, \qquad \mathbf{U}(x>0, t=0) = \mathbf{U}_R,$$

there exists a solution consisting of K nonlinear waves, where K is the number of equations in the system. This is shown schematically in Fig. 2 for the Euler equations (3). The solution is self-similar; $\mathbf{U}$ is a function only of $\eta = x/t$. For the equations of gasdynamics, a unique solution always exists as long as a vacuum does not form (see Chapter 18 of Smoller [9]).

Godunov uses the Riemann problem to compute the flux in the following way.

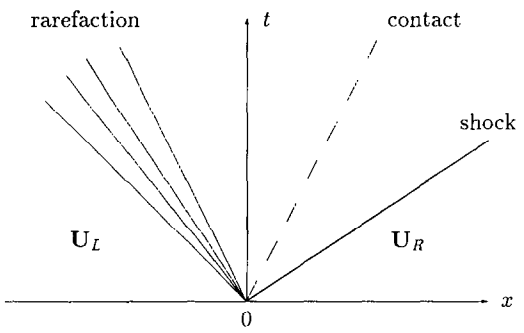

FIG. 2. Riemann problem for the Euler equations.

For the interface between cells j and $j+1$, he solves the Riemann problem with $\mathbf{U}_L = \mathbf{U}_j^n$, $\mathbf{U}_R = \mathbf{U}_{j+1}^n$. The flux is then given by the state at $\eta = 0$, i.e.,

$$\hat{\mathbf{F}} = \mathbf{F}(\mathbf{U}(\eta = 0)).$$

This flux may be written in the following way: define

$$\Delta\mathbf{F}^+ = \mathbf{F}_R - \mathbf{F}(\mathbf{U}(\eta = 0)), \qquad \Delta\mathbf{F}^- = -\mathbf{F}_L + \mathbf{F}(\mathbf{U}(\eta = 0)),$$

which gives $\Delta\mathbf{F} = \mathbf{F}_R - \mathbf{F}_L = \Delta\mathbf{F}^+ + \Delta\mathbf{F}^-$. One can think of $\Delta\mathbf{F}^\pm$ as being the contributions to $\Delta\mathbf{F}$ due to the right and left running waves at the interface, respectively. The flux may then be written as

$$\hat{\mathbf{F}} = \tfrac{1}{2}(\mathbf{F}_R + \mathbf{F}_L) - \tfrac{1}{2}(\Delta\mathbf{F}^+ - \Delta\mathbf{F}^-). \tag{6}$$

It is this form of the flux funtion that gives rise to the term "flux difference splitting." Both Roe's and Osher's schemes, presented below, may be written in this form.

One disadvantage of Godunov's flux formula is that the Riemann problem leads to a set of nonlinear algebraic equations which must be solved iteratively. Both Roe's and Osher's schemes are designed to overcome this problem by making use of approximations to the solution of Riemann's problem that result in explicit, noniterative expressions for the flux function in Eq. (5). These methods are now discussed.

3.2. *Roe's Scheme*

Roe [5] approximately solves the Riemann problem for two adjacent states, $\mathbf{U}_L$, $\mathbf{U}_R$, by finding a mean Jacobian matrix $\tilde{\mathbf{A}}(\mathbf{U}_L, \mathbf{U}_R)$ that satisfies the identity,

$$\Delta\mathbf{F} = \tilde{\mathbf{A}}\,\Delta\mathbf{U}, \tag{7}$$

where $\Delta(\ ) = (\ )_R - (\ )_L$. Roe requires $\tilde{\mathbf{A}}$ to have a complete set of eigenvalues and right eigenvectors and to satisfy $\tilde{\mathbf{A}}(\mathbf{U}, \mathbf{U}) = \partial\mathbf{F}/\partial\mathbf{U}$ (i.e., it reduces to the exact

Jacobian when $\mathbf{U}_L = \mathbf{U}_R$). He refers to these requirements collectively as "Property U."

Let $\tilde{\lambda}^{(k)}$, $\tilde{\mathbf{r}}^{(k)}$, and $\alpha^{(k)}$ be the kth eigenvalue, right eigenvector, and inner product of the left eigenvector with $\Delta\mathbf{U}$, respectively. Equation (7) can be rewritten in terms of these quantities,

$$\Delta\mathbf{F} = \sum_{k=1}^{K} \tilde{\mathbf{r}}^{(k)} \tilde{\lambda}^{(k)} \alpha^{(k)},$$

where K is the number of equations. Because of the identity Eq. (7), this expression for the flux difference is exact when the left and right states are connected by a discontinuity satisfying the Rankine–Hugoniot jump conditions. In that case, $\Delta\mathbf{U}$ projects onto the appropriate right eigenvector $\tilde{\mathbf{r}}^{(k)}$ of $\tilde{\mathbf{A}}$. Thus $\alpha^{(i)} = 0$, $i \neq k$, and the speed of the discontinuity is equal to the corresponding eigenvalue $\tilde{\lambda}^{(k)}$.

A first-order accurate Riemann flux at the interface between cells R and L is given by

$$\hat{\mathbf{F}} = \tfrac{1}{2}(\mathbf{F}_R + \mathbf{F}_L) - \tfrac{1}{2} \sum_{k=1}^{K} \tilde{\mathbf{r}}^{(k)} |\tilde{\lambda}^{(k)}| \alpha^{(k)}. \tag{8}$$

The expressions for $\tilde{\lambda}^{(k)}$, $\tilde{\mathbf{r}}^{(k)}$, and $\alpha^{(k)}$ for Eq. (3) have been given by Roe [5]. The corresponding expressions for the isothermal Euler equations (2) are given in Appendix A.

3.3. *Osher's Scheme*

Osher's [6] approach to the Riemann problem is to consider the problem in the state space rather than the physical space. The flux difference between the left and the right states may be written

$$\mathbf{F}_R - \mathbf{F}_L = \int_{\mathbf{U}_L}^{\mathbf{U}_R} \frac{\partial \mathbf{F}}{\partial \mathbf{U}} \, d\mathbf{U}, \tag{9}$$

where the integral is evaluated along an arbitrary path Γ in the state space. Assume the eigenvalues of $\partial\mathbf{F}/\partial\mathbf{U}$ are ordered from smallest to largest, i.e., $\lambda^{(1)} \leqslant \lambda^{(2)} \leqslant \cdots \leqslant \lambda^{(K)}$. Osher chooses a particular path from $\mathbf{U}_L$ to $\mathbf{U}_R$ that consists of a K-simple wave, followed by a $(K-1)$-simple wave, and so on to 1-simple wave. This wave path is uniquely determined by the left and right states. If we take $d\alpha^{(k)}$ to be the inner product of the kth left eigenvector of $\partial\mathbf{F}/\partial\mathbf{U}$ with $d\mathbf{U}$, then along a k-simple wave, $d\alpha^{(i)} = 0$, $i \neq k$. The path integral for $\Delta\mathbf{F} = \mathbf{F}_R - \mathbf{F}_L$ may be written

$$\Delta\mathbf{F} = \sum_{k=1}^{K} \int_{\Gamma^{(k)}} \mathbf{r}^{(k)} \lambda^{(k)} \, d\alpha^{(k)},$$

where $\mathbf{r}^{(k)}$ and $\lambda^{(k)}$ are the kth right eigenvector and eigenvalue, respectively, and

$\Gamma^{(k)}$ is that portion of the path along the k-simple wave. Osher's first-order accurate numerical flux is

$$\hat{\mathbf{F}} = \tfrac{1}{2}(\mathbf{F}_R + \mathbf{F}_L) - \tfrac{1}{2} \sum_{k=1}^{K} \int_{\Gamma^{(k)}} \mathbf{r}^{(k)} |\lambda^{(k)}| \, d\alpha^{(k)}. \tag{10}$$

Note the formal similarity between Eqs. (8) and (10).

The evaluation of Eq. (10) requires knowledge only of the states connecting the $\Gamma^{(k)}$ and $\Gamma^{(k+1)}$ subpaths, and of any sonic states that occur along each subpath. For the Euler equations, these states can be computed explicitly from knowledge of the left and right states, so that no iterations are required. In Osher and Solomon [6], formulas for these intermediate states are given for the Euler equations (3). Expressions for the intermediate states for the isothermal Euler equations (2) are presented in Appendix B.

4. Results

Solutions for the model problem described in Section 2 are shown below. In all cases, the solutions are shown after approximately 2000 time steps, after which the shock has crossed about 40 cells.

The solution to Burgers equation can be seen in Fig. 3. Since there are no rarefactions, Roe's scheme is identical to Godunov's scheme for this problem. Osher's scheme reduces to the Engquist–Osher scheme for scalar equations. There is not much to be said, other than to note that both solutions behave as expected. The shock profiles are monotone. Roe's (Godunov's) scheme gives a shock with a single internal zone, while Engquist–Osher gives a two-zone shock.

More interesting results are obtained for the isothermal Euler equations (2). The left and right states have been chosen to give about an order of magnitude pressure rise across the shock. Solutions obtained using Roe's and Osher's schemes are compared in Fig. 4. The plots show the Riemann invariants of the equations,

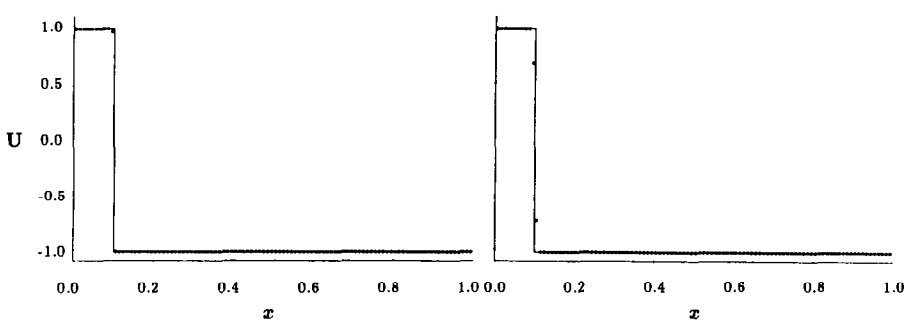

FIG. 3. Burgers equation solution: Roe's/Godunov's (left); Engquist–Osher (right).

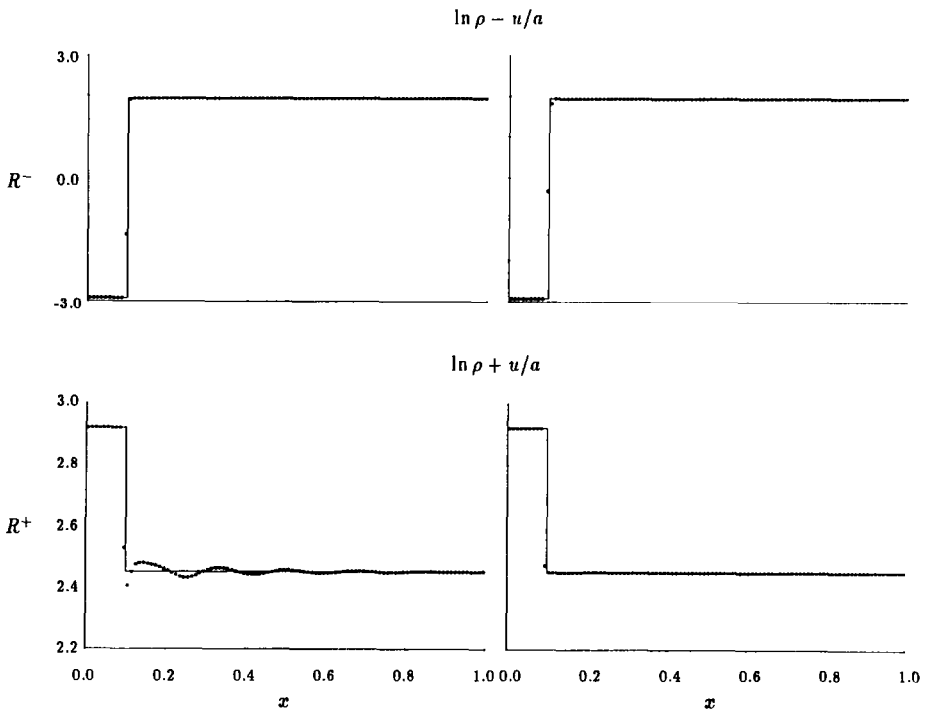

FIG. 4. Isothermal Euler equations: Roe's scheme (left); Osher's scheme (right).

$(\ln \rho \pm u/a)$, associated with the $u \pm a$ characteristics, respectively. The $(\ln \rho - u/a)$ invariant is a characteristic variable belonging to the shock family and behaves qualitatively in the same way as the solution of Burgers equations. Both schemes have monotone profiles in this invariant. However, in the downstream running wave family, represented by the $(\ln \rho + u/a)$ invariant, there is a smooth, long wavelength error behind the shock. The wavelength of this error is $\sim 15\,\Delta x$. This

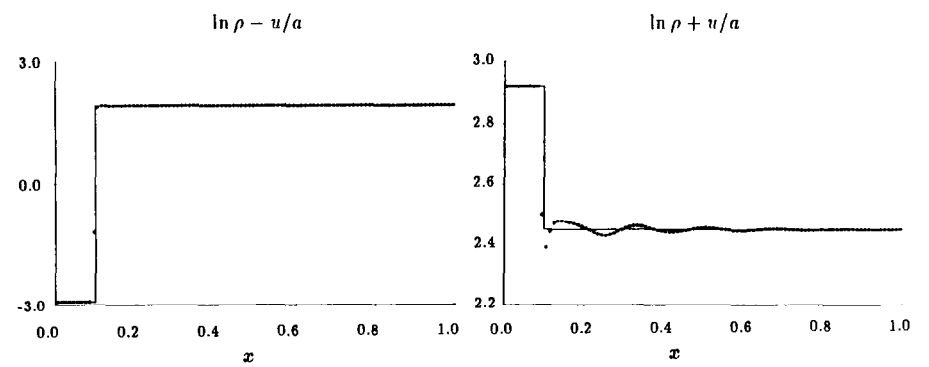

FIG. 5. Isothermal Euler equations, Godunov's scheme.

corresponds very nearly to the value of $(u + a)\,\Delta x/s$ behind the shock, where s is the shock speed, for the parameters of this problem. The wavelength and amplitude are insensitive to changes of the Courant number. The error is particularly pronounced for Roe's scheme. Although the error is also present in Osher's scheme, it is small enough to be negligible. Because the error has such a long wavelength it is only slowly damped by the dissipation of the scheme, even though the method is only first-order accurate.

The solution to this problem using Godunov's method is shown in Fig. 5. These results are virtually indistinguishable from those obtained using Roe's scheme. This

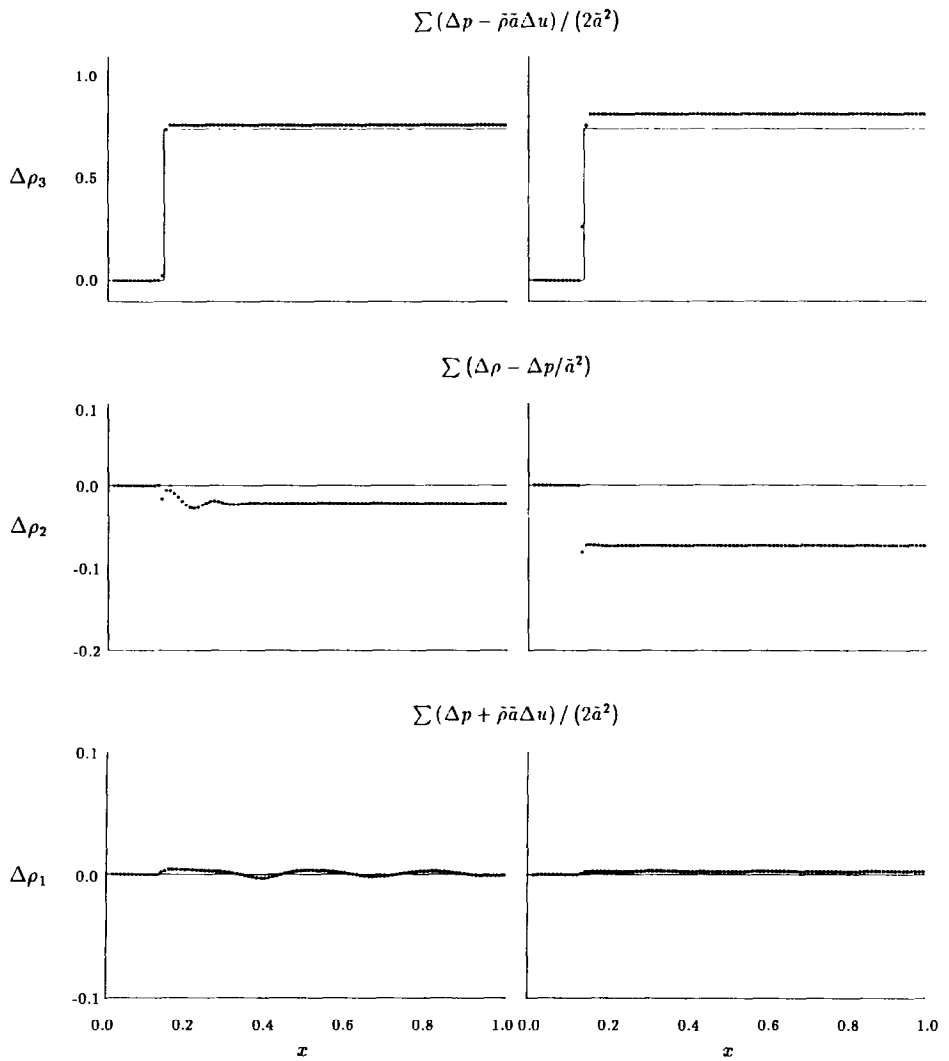

FIG. 6. Full Euler equations: Roe's scheme (left); Osher's scheme (right).

is expected, since the differences in Roe's approximate Riemann solver and an exact Riemann solver are small near a shock (and vanish completely if the jump conditions are satisfied across two cells).

For the full Euler equations, as for the isothermal equations, the left and right states have been chosen to give about a one order of magnitude pressure rise acorss the shock (a shock Mach number $M_s = 3$). For this system of equations, we no longer have the integrability conditions along the characteristics that give us Riemann invariants as in the isothermal case. To plot the results, we need some other measure of the wave strengths. Roe's linearization at cell interfaces provides us with a convenient choice:

$$\sum \frac{1}{2\tilde{a}^2}(\Delta p - \tilde{\rho}\tilde{a}\,\Delta u), \qquad \tilde{u} - \tilde{a};$$

$$\sum \left(\Delta \rho - \frac{\Delta p}{\tilde{a}^2}\right), \qquad \tilde{u};$$

$$\sum \frac{1}{2\tilde{a}^2}(\Delta p + \tilde{\rho}\tilde{a}\,\Delta u), \qquad \tilde{u} + \tilde{a};$$

where the summation is from 0 to j. This is a discrete analog of integrating the characteristic variables from the inlet to cell j and remains valid across shocks. This allows us to decouple the wave families for plotting purposes. In the results shown in Fig. 6 we can see, as in the isothermal case, that the wave family associated with the shock is monotone, but there is again a long wavelength noise behind the shock in the downstream running waves (the u and $u + a$ families). The amplitude of the error is largest in the entropy wave, but the wavelength of the error is much longer in the acoustic wave. As with the isothermal equations, the observed wavelengths of the errors in the entropy and acoustic waves correspond quite well to $u\,\Delta x/s$ and $(u + a)\,\Delta x/s$, respectively. Once again we see that the amplitude of the noise is hardly noticeable for Osher's scheme, while the error is a few percent of the postshock density with Roe's scheme. The results obtained with Godunov's scheme are not shown; as with the isothermal Euler equations, they scarcely differ from the results given by Roe's scheme.

5. Discussion

From the results shown in Section 4, it is seen that there is a source of numerical error that occurs when computing nearly stagnant shocks using flux difference splitting methods. This error has been observed and discussed previously by Colella and Woodward [4, 2] in the context of extremely strong (pressure ratios $\sim 10^5$ or greater) shocks. However, the results shown above were for much weaker shocks, and the author has observed this phenomenon even for transonic (pressure ratio ~ 1.2) shocks. It is also important to note that the error only occurs with nonlinear

systems of equations. Shocks for the scalar inviscid Burgers equation (1) are perfectly well behaved.

In [4], Colella and Woodward discuss this problem in some detail for Godunov's scheme. Their explanation boils down to this: the dissipation in this method scales as the eigenvalue (wave speed) of the appropriate characteristic field. At a slowly moving shock, the dissipation for the characteristic variable that jumps across the shock necessarily becomes very small. Thus, the shock transition layer is too thin, in the sense that there is insufficient dissipation to ensure the correct entropy production in the shock. From this argument, they conclude that additional dissipation must be added to the scheme at a shock. They go on to present several artificial viscosity models to alleviate the problem.

The problem with Colella and Woodward's explanation is that it does not explain why scalar equations are well behaved, since the dissipation at a slow shock is small in that case as well. Furthermore, the noise seen with systems of equations shows up in the downstream running waves, for which the dissipation does not vanish; the characteristic variable associated with the shock has monotone behavior. Following a line of reasoning suggested by P. L. Roe (private communication), the error can be explained in terms of the discrete shock structure.

First consider Roe's scheme, since the idea can be explained most easily using his flux function. Assume that the shock is a 1-shock (left running) to correspond with the computations presented in the previous section. The same arguments will apply to a right running shock. A schematic of discrete shock transition layer is shown in Fig. 7. We wish to find conditions that will guarantee that no noise will be generated in the downstream running wave families. Let $\mathbf{U}^n_{j+1} = \mathbf{U}_R$, the postshock state; then $\mathbf{U}^n_j$ is the last internal zone of the shock. If no noise is generated, then

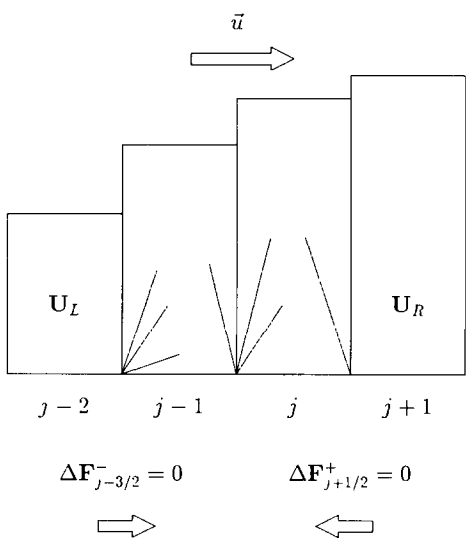

FIG. 7. Schematic of the discrete shock transition layer.

the strengths of the downstream running waves must vanish, which means that in Eq. (8),

$$\alpha^{(1)} \neq 0, \qquad \alpha^{(k)} = 0 \qquad \text{for} \quad k \neq 1.$$

This is equivalent to requiring that $\mathbf{U}_j^n$ and $\mathbf{U}_{j+1}^n$ are connected by a 1-shock. Since this must continue to hold for all subsequent time, the internal shock zone $\mathbf{U}_j$ must move smoothly along the shock curve (the Hugoniot curve of shock adiabatic for the full Euler equations) passing through $\mathbf{U}_R$ until it reaches the postshock state.

In the scalar case, the above restriction is automatically satisfied, since any state between $\mathbf{U}_L$ and $\mathbf{U}_R$ can be connected to the latter by a 1-shock. There is no downstream running wave family in which any noise can appear, so the shock is well behaved.

Consider the problem in state space. Let $H(\mathbf{U}; \mathbf{U}_R) = 0$ be the equation of the shock curve passing through $\mathbf{U}_R$. Also, let ∇_U be the gradient operator with respect to the state vector $\mathbf{U}$. Using the flux function in the form Eq. (6), we may rewrite Eq. (5) in the form

$$\delta \mathbf{U}_j^n = \mathbf{U}_j^{n+1} - \mathbf{U}_j^n = -\frac{\Delta t}{\Delta x}(\Delta \mathbf{F}_{j+1/2}^- + \Delta \mathbf{F}_{j-1/2}^+). \tag{11}$$

If $\mathbf{U}_j^n$ lies on the shock curve, then $H(\mathbf{U}_j^n; \mathbf{U}_R) = 0$, and we require

$$\nabla_U H(\mathbf{U}_j^n; \mathbf{U}_R) \cdot \delta \mathbf{U}_j^n = 0.$$

This may be rewritten, using Eq. (11), as

$$\nabla_U H(\mathbf{U}_j^n; \mathbf{U}_R) \cdot (\Delta \mathbf{F}_{j+1/2}^- + \Delta \mathbf{F}_{j-1/2}^+) = 0. \tag{12}$$

This expression involves $\mathbf{U}_{j-1}^n$, and clearly leads to restrictions on the internal structure of the shock. Whether or not Eq. (12) is satisfied obviously depends upon the choice of the numerical flux function.

It is easy to see that no shock with only a one zone transition may satisfy Eq. (12). Consider such a transition: let $\mathbf{U}_j^n$ be the internal zone of the discrete shock, and $\mathbf{U}_{j+1}^n = \mathbf{U}_R$, $\mathbf{U}_{j-1}^n = \mathbf{U}_L$. There can be no right running waves at $j + \frac{1}{2}$, no left running waves at $j - \frac{1}{2}$. Thus Eq. (12) becomes

$$\nabla_U H(\mathbf{U}_j^n; \mathbf{U}_R) \cdot (\mathbf{F}_R - \mathbf{F}_L) = 0, \tag{13}$$

which from the jump relations $\Delta \mathbf{F} = s\, \Delta \mathbf{U}$ gives

$$\nabla_U H(\mathbf{U}_j^n; \mathbf{U}_R) \cdot (\mathbf{U}_R - \mathbf{U}_L) = 0, \qquad s \neq 0. \tag{14}$$

In other words the shock curve $H = 0$ must be everywhere tangent to $\mathbf{U}_R - \mathbf{U}_L$, which clearly is not true for a general nonlinear system of equations (including the isothermal and full Euler equations). Thus no one point unsteady shock profile exists in this case. This contrasts with the situation for steady shocks, for which

Godunov's and Roe's schemes do yield a one-parameter family of shocks with a single transition zone (because $\mathbf{F}_R = \mathbf{F}_L$ and Eq. (13) is satisfied identically). We can also see that Colella and Woodward's argument that Godunov's scheme gives too narrow a shock is in a sense correct.

Although Roe's scheme was considered above, Eq. (12) applies as well to Godonov's scheme with an exact Riemann solver, or to *any* approximate Riemann solver that is exact at a Rankine–Hugoniot jump. In fact, such a Riemann solver will exhibit the same behavior as Roe's or Godunov's schemes at a slow shock. For Osher's scheme, the left and right states of the shock are connected by a compound simple wave path, and so $\mathbf{U}_j^n$ must lie on the 1-simple wave passing through $\mathbf{U}_R$. In this case, the relation $H = 0$ should be taken to represent this 1-simple wave, rather than the shock curve, and Eq. (12) still applies. The 1-simple wave and the shock curve meet very smoothly at $\mathbf{U}_R$, with the same first and second derivatives. Near the postshock state, the difference between the two curves is thus quite small.

We can see now why Osher's scheme performs so much better than Roe's or Godunov's schemes at a slow shock. Osher evaluates Eq. (9) along a path Γ in state space that lies close to the shock curve. Because $\Delta\mathbf{F}^{\pm}$ are evaluated along a path that so nearly satisfies $H = 0$, the internal states of the shock cannot deviate much from this path, and the amplitude of the noise in the downstream running waves remains very small. Note that it is not only Osher's use of a differentiable flux function that leads to such good performance; his choice of wave path Γ is as important.

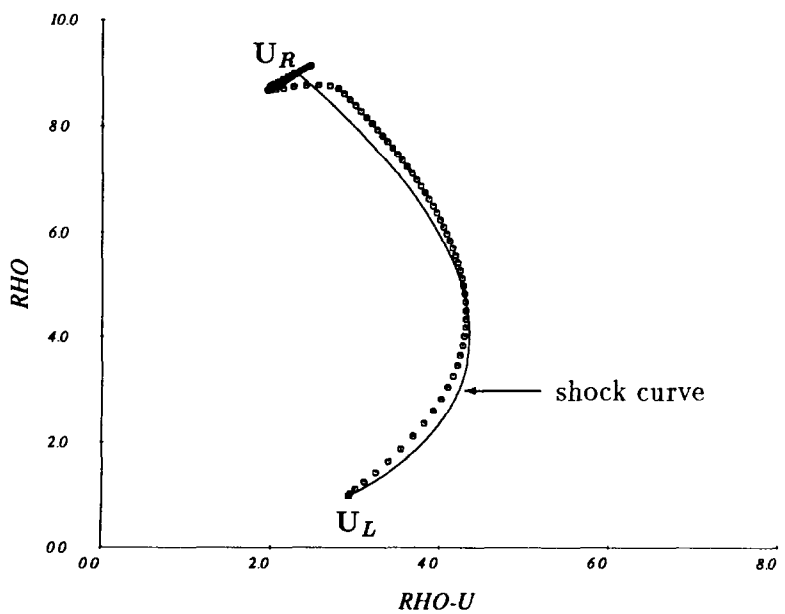

FIG. 8. Unsteady shock structure, Roe's scheme.

To illustrate these points, the isothermal Euler equations (2) are considered, and the computed unsteady shock structure is examined. In Fig. 8, the evolution of the internal shock structure in the state space $(\rho, \rho u)^T$ is shown for the first-order computation presented in Section 4. The solid line is the shock curve connecting the left and right states. The symbols show the evolution of the internal zone starting at $\mathbf{U}_L$ and passing through the shock to $\mathbf{U}_R$. The path is smooth, but deviates considerably from $H=0$ as it approaches the postshock state. The "knee" in the curve occurs after approximately 50 time steps, at which time the shock has completely crossed one cell. The large error in the postshock state is obvious, as is the subsequent oscillation behind the shock. These results are not significantly different from Godunov's scheme (not shown).

From Fig. 8 we can also see a direct geometric proof that a one-point shock transition cannot exist in general. If we have such a shock profile, the internal zone at time n must lie on the shock curve $H=0$. The difference equation for this shock point may be written as $\delta \mathbf{U}_j^n = -s\,\Delta t/\Delta x(\mathbf{U}_R - \mathbf{U}_L)$. Advancing to time level $n+1$, the point must move parallel to $\mathbf{U}_R - \mathbf{U}_L$, which is the straight line between the endpoints of the shock curve in Fig. 8. It is immediately seen that this line is not tangent to $H=0$, in general, so the point must move off the shock curve, i.e., Eq. (14) is not satisfied.

In Fig. 9, the shock given by Osher's scheme is presented. The compound wave path between the pre- and postshock states is shown and lies to the left of the shock curve. The shock is thicker with Osher's scheme, so it takes longer for it to cross

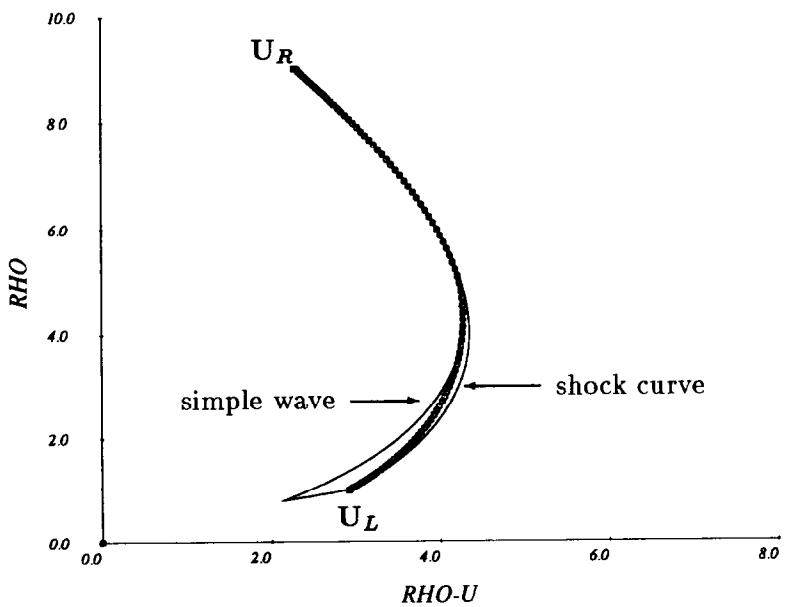

FIG. 9. Unsteady shock structure, Osher's scheme.

a cell. Note that the internal zone passes smoothly to the 1-simple wave path and always lies between the simple wave path and the shock curve.

Closer inspection of the results reveals that the intermediate states used in evaluating Osher's flux function Eq. (10) tend to lie between the simple wave path and the shock curve in state space and hence remain close to the shock curve. By contrast, Roe's approximate (as well as an exact) Riemann solver gives intermediate states that can lie quite far from the shock curve. Small changes in an internal state of the shock lead to relatively large changes in the solution of the Riemann problem, making $\Delta \mathbf{F}^{\pm}$ sensitive to small errors. Osher's use of a differentiable flux function, in which the path integral Eq. (9) always includes the sonic state, as well as a choice of path that lies close to the shock curve, is the reason for its better performance here.

To show the importance of the ordering of the wave paths in Osher's scheme, a computation for Eq. (2) was performed in which the order of the paths was reversed. (This is intuitively the "correct" ordering, although in general the flux function is still multivalued in the physical space.) Results are shown in Fig. 10. The wave path now lies very far from the shock curve, and the deviation is greatest at the downstream side of the shock. At least one intermediate state in the evaluation of Eq. (10) lies on the 1-simple wave curve to the right. Small changes in the internal shock states lead to larger changes in the intermediate states, so that the

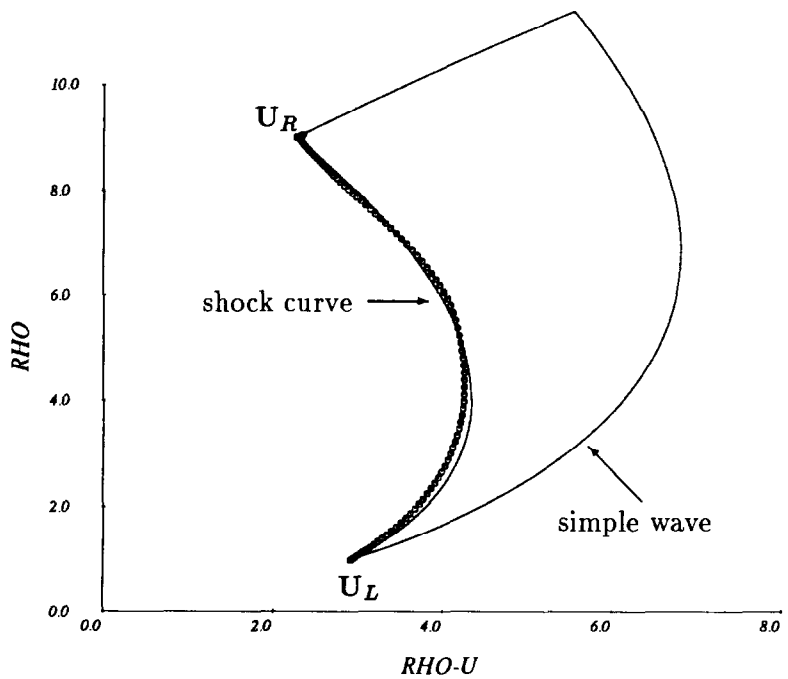

FIG. 10. Unsteady shock structure, Osher's scheme, inverted wave path order.

$\Delta \mathbf{F}^{\pm}$ are more sensitive to errors. The Riemann invariants are shown in Fig. 11; note that the performance has degraded (although it is still better than Roe's or Godunov's schemes).

The most important consequence of the error analyzed here occurs when higher order accuracy is obtained through the use of TVD flux limiters. Since the TVD property (which strictly applies only to scalar equations) depends upon the underlying first-order accurate scheme being truly monotone, and because the error in this case is so smooth, the noise generated at the shock is preserved for longer distances downstream. Thus the problem is accentuated by the use of flux limiting.

This point is illustrated in Fig. 12, in which a solution to Eq. (2) using Roe's second-order accurate TVD scheme is shown. The "minmod" flux limiter was used. It is easily seen that noise in the downstream running wave family is now preserved for an even longer distance than in the first-order solution of Fig. 4. Note that the $(\ln \rho - u/a)$ Riemann invariant is still monotone. Further illustrations of this behavior have been shown by Woodward and Colella [2], who clearly demonstrate how this can affect the global accuracy in unsteady calculations.

As mentioned in the Introduction, the error analyzed here may be a contributing factor to the slow convergence to steady state seen by Lytton [7] and Yee [8]. Both these researchers use higher order TVD schemes based on Roe's approximate Riemann solver. In particular, Yee reports difficulty for steady state computations at Mach numbers >4. It is worth noting that she finds the convergence rate to be sensitive to the size of her "entropy enforcement parameter," which is simply an artificial viscosity added at sonic points and shocks. Increasing the viscosity improves the convergence rate. Since this should increase the shock thickness and reduce the postshock error in the same way that Colella and Woodward's [4] additional dissipation terms do, it is consistent with the error observed in this work. In two dimensions, one can speculate that the problem may be accentuated by shocks skew to the mesh lines and the nonlinearity of the flux limiters. These factors could result in shocks which never quite become steady.

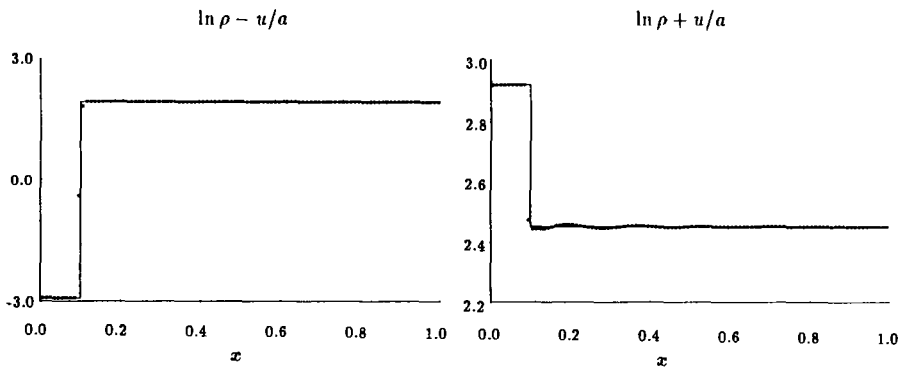

FIG. 11. Isothermal Euler equations, Osher's scheme, inverted wave path order.

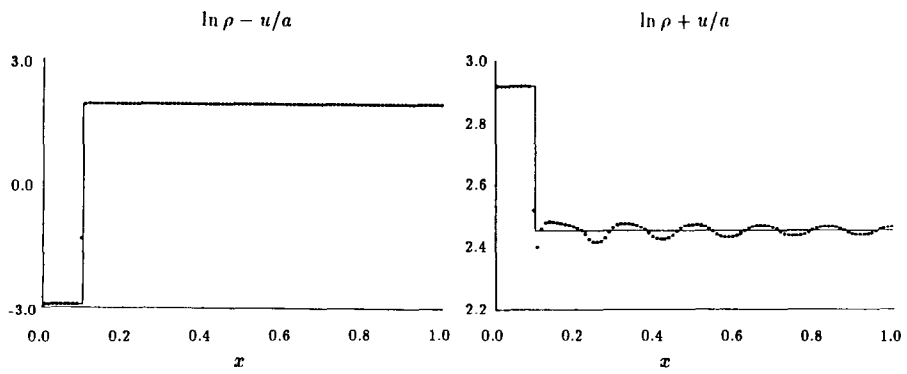

FIG. 12. Isothermal Euler equations, Roe's scheme using the "minmod" flux limiter.

The results of this study also raise an interesting question concerning shock capturing schemes. The attractive property of an exact Riemann solver, or Roe's approximate Riemann solver, is that they "recognize" shocks. That is, if two adjacent states satisfy the Rankine–Hugoniot conditions, they are treated as a shock. In practice, however, the numerical shock will have some thickness, so the flux function cannot "see" the whole of it. Osher's approximate Riemann solver, on the other hand, never connects two states by a shock. As a result, the numerical shock is thicker, but at least for the cases shown here it is better behaved. It may be that there are some advantages to treating captured shocks using flux formulas that do not recognize the analytic shock jump conditions. The alternative is either to tolerate some postshock noise which may corrupt the solution in certain cases, or to add more numerical dissipation as Colella and Woodward suggest [4]. In the latter case, the shock resolution is degraded anyway.

A final point must be made regarding a "fast" shock, where the eigenvalues do not change sign across the shock. In this case, the straight line between the left and right states in the state space is more nearly aligned with the shock curve connecting them. Hence the deviations between the internal shock states satisfying Eq. (12) and the actual states will be much smaller than for the slow shock case. In addition, any postshock noise will be of short wavelength and will be effectively damped by the dissipation of the scheme.

6. CONCLUSIONS

To summarize, there are two main conclusions to the present work. First, for slowly moving shocks, some flux difference splitting schemes yield significant error behind the shock. This noise cannot be eliminated by appealing to TVD concepts and may be a contributing factor to the slow convergence to steady state observed for such schemes. Second, this error can be explained in terms of the discrete shock

structure of the particular scheme and suggests that numerical flux formulas that recognize a Rankine–Hugoniot jump may be less suitable for shock capturing than differentiable flux formulas, at least under certain conditions.

APPENDIX A: EIGENVECTORS AND EIGENVALUES FOR ROE'S SCHEME FOR THE ISOTHERMAL EULER EQUATIONS

For the isothermal Euler equations (2), Roe's mean value Jacobian matrix is computed from the averages

$$\tilde{\rho} = (\rho_R \rho_L)^{1/2},$$

$$\tilde{u} = \frac{\rho_R^{1/2} u_R + \rho_L^{1/2} u_L}{\rho_R^{1/2} + \rho_L^{1/2}}.$$

These are also the values of $\tilde{\rho}$ and $\tilde{u}$ for the full Euler equations (3) (see Roe [5]). The eigenvalues, right eigenvectors, and inner product of the left eigenvectors with $\Delta \mathbf{U}$ are

$$\tilde{\lambda}^{(1)} = \tilde{u} - a, \qquad \tilde{\mathbf{r}}^{(1)} = \begin{pmatrix} 1 \\ \tilde{u} - a \end{pmatrix}, \qquad \alpha^{(1)} = \frac{1}{2}\left(\Delta\rho - \frac{\tilde{\rho}}{a}\Delta u\right),$$

$$\tilde{\lambda}^{(2)} = \tilde{u} + a, \qquad \tilde{\mathbf{r}}^{(2)} = \begin{pmatrix} 1 \\ \tilde{u} + a \end{pmatrix}, \qquad \alpha^{(2)} = \frac{1}{2}\left(\Delta\rho + \frac{\tilde{\rho}}{a}\Delta u\right).$$

It may be readily verified that these averages satisfy Eq. (7) and Roe's "Property *U*."

APPENDIX B: EVALUATION OF THE PATH INTEGRAL IN OSHER'S SCHEME FOR THE ISOTHERMAL EULER EQUATIONS

The path integral Eq. (9) required for Osher's scheme is easily evaluated for the isothermal Euler equations (2). From the left state $\mathbf{U}_L$ a 2-simple wave is followed to an intermediate state $\mathbf{U}_I$, which is followed by a 1-simple wave to $\mathbf{U}_R$. Both wave families are genuinely nonlinear. Thus there can be at most one change of sign of $\lambda^{(2)} = u + a$ between $\mathbf{U}_L$ and $\mathbf{U}_I$. Similarly, $\lambda^{(1)} = u - a$ can change sign at no more than one point along the 1-simple wave path from $\mathbf{U}_I$ to $\mathbf{U}_R$. These two sonic points are called $\mathbf{U}_{S,L}$ and $\mathbf{U}_{S,R}$, respectively. The three intermediate states are all that are needed to evaluate the numerical flux function Eq. (10).

To compute $\mathbf{U}_{S,L}$, $\mathbf{U}_I$, and $\mathbf{U}_{S,R}$, the following relationships are used: along the 2-simple wave,

$$\lambda^{(2)} = u + a, \qquad d\alpha^{(1)} = d\left(\ln \frac{\rho}{\rho_{\text{ref}}} - \frac{u}{a}\right) = 0;$$

along the 1-simple wave,

$$\lambda^{(1)} = u - a, \qquad d\alpha^{(2)} = d\left(\ln \frac{\rho}{\rho_{\text{ref}}} + \frac{u}{a}\right) = 0,$$

where ρ_{ref} is some arbitrary reference density.

With the above relations, the following values for the density and velocity at the intermediate states are found to be

$$\rho_{S,L} = \rho_L \exp\left(-1 - \frac{u_L}{a}\right),$$

$$u_{S,L} = -a,$$

$$\rho_I = (\rho_L \rho_R)^{1/2} \exp\left(\frac{u_R - u_L}{2a}\right),$$

$$u_I = \frac{a}{2} \ln \frac{\rho_R}{\rho_L} + \frac{u_R + u_L}{2},$$

$$\rho_{S,R} = \rho_R \exp\left(-1 + \frac{u_R}{a}\right),$$

$$u_{S,R} = a.$$

If we introduce the terms,

$$\sigma_L = \operatorname{sgn}(\lambda_L^{(2)}),$$

$$\sigma_{I,L} = \operatorname{sgn}(\lambda_I^{(2)}),$$

$$\sigma_{I,R} = \operatorname{sgn}(\lambda_I^{(1)}),$$

$$\sigma_R = \operatorname{sgn}(\lambda_R^{(1)}),$$

where the function $\operatorname{sgn}(x)$ returns ± 1 if x is positive or negative, respectively, then Osher's flux formula (10) may be written

$$\hat{\mathbf{F}} = \tfrac{1}{2}(\mathbf{F}_R + \mathbf{F}_L) - \tfrac{1}{2}[\sigma_R(\mathbf{F}_R - \mathbf{F}_{S,R}) + \sigma_{I,R}(\mathbf{F}_{S,R} - \mathbf{F}_I) + \sigma_{I,L}(\mathbf{F}_I - \mathbf{F}_{S,L}) + \sigma_L(\mathbf{F}_{S,L} - \mathbf{F}_L)].$$

REFERENCES

1. P. L. ROE, *Ann. Rev. Fluid Mech.* **18**, 337 (1986).
2. P. WOODWARD AND P. COLELLA, *J. Comput. Phys.* **54**, 115 (1984).
3. S. K. GODUNOV, *Mat. Sb.* **47**, 271 (1959).
4. P. COLELLA AND P. R. WOODWARD, *J. Comput. Phys.* **54**, 174 (1984).
5. P. L. ROE, *J. Comput. Phys.* **43**, 357 (1981).
6. S. OSHER AND F. SOLOMON, *Math. Comput.* **38**, 339 (1982).
7. C. C. LYTTON, *J. Comput. Phys.* **73**, 395 (1987).
8. H. C. YEE, Upwind and symmetric shock-capturing schemes, NASA TM-89464, May 1987 (unpublished).
9. J. SMOLLER, *Shock Waves and Reaction-Diffusion Equations* (Springer-Verlag, New York, 1983).